# Inorganic Chemistry

## including bioinorganic chemistry

September 2, 2013
Volume 52, Number 17
pubs.acs.org/IC

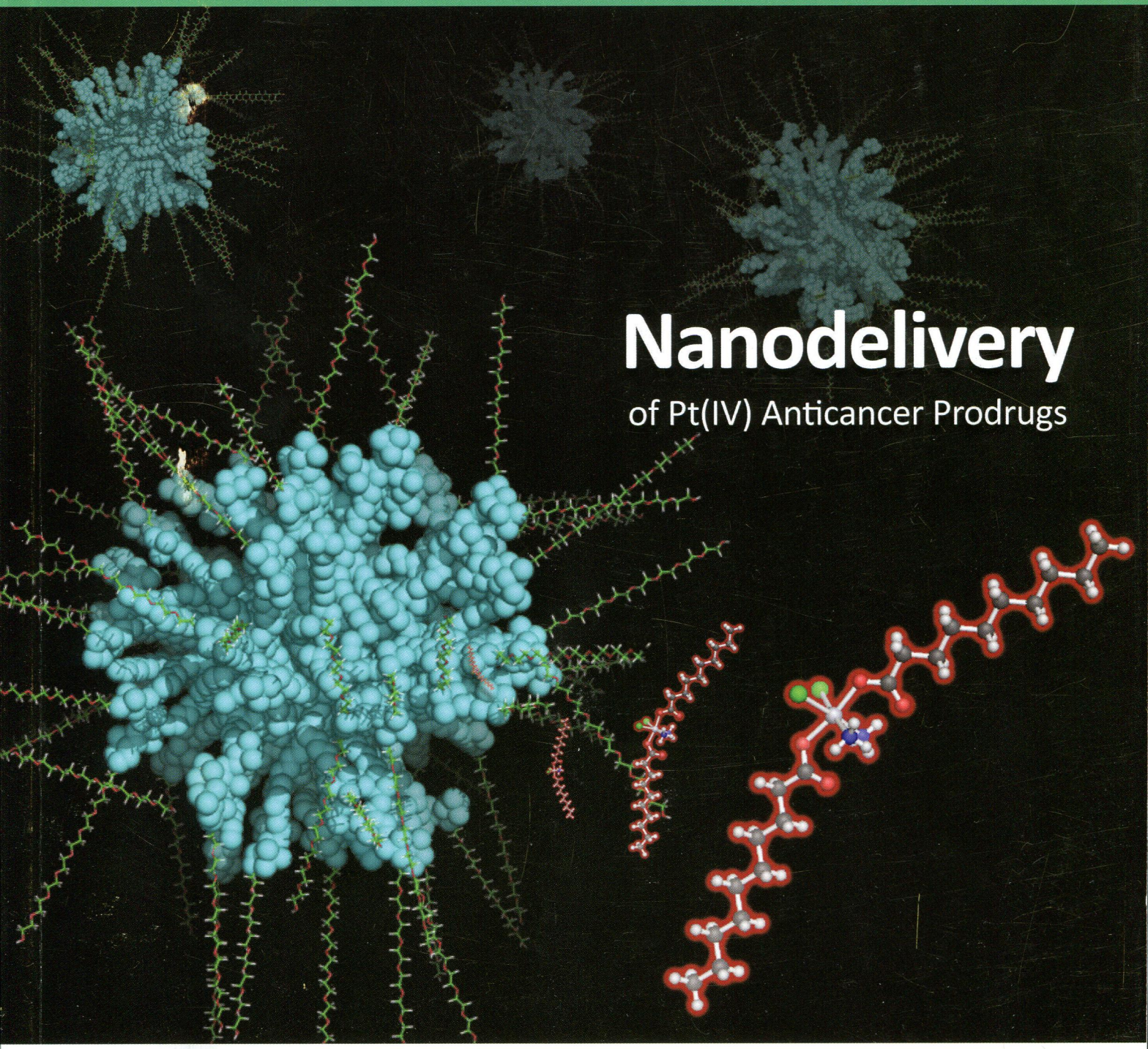


ACS Publications
MOST TRUSTED. MOST CITED. MOST READ.

www.acs.org

Inorganic Chemistry

SEPTEMBER 2, 2013
VOLUME 52 ISSUE 17

INOCAJ 52(17) 9699–10216 (2013)
ISSN 0020-1669
Registered in the U.S. Patent and Trademark Office


**ON THE COVER:** A stylized depiction of a micelle composed of amphiphilic block copolymers, in which the hydrophobic cores are shown in space-filling mode and the hydrophobic shells as sticks. Emanating from the foremost particle is *cis,cis,trans*-$[Pt(NH_3)_2Cl_2(O_2C(CH_2)_8CH_3)_2]$, a Pt(IV) prodrug designed to be encapsulated within the micellar core. See T. C. Johnstone and S. J. Lippard, p 9915.

## Communications



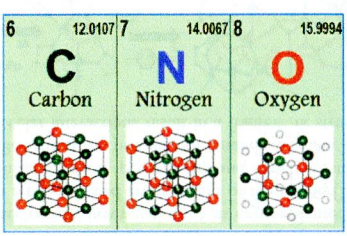




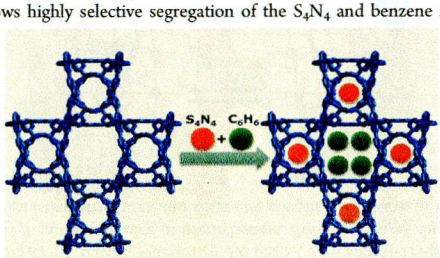

9705 S dx.doi.org/10.1021/ic401122u

**Nonporous Titanium–Oxo Molecular Clusters That Reversibly and Selectively Adsorb Carbon Dioxide**

Keunil Hong and Hyungphil Chun*

Titanium(IV) oxocarboxylate clusters are potential molecular adsorbents with high thermal and chemical stabilities. The nonporous clusters with rigid side groups show selective sorption for carbon dioxide, unlike their porous cousin.

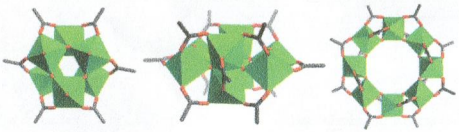

9708 S dx.doi.org/10.1021/ic401281x

**Fate of a Giant $\{Mo_{72}Fe_{30}\}$-Type Polyoxometalate Cluster in an Aqueous Solution at Higher Temperature: Understanding Related Keplerate Chemistry, from Molecule to Material**

Raju Mekala, Sabbani Supriya,* and Samar K. Das*

If an aqueous solution of the well-known giant $\{Mo_{72}Fe_{30}\}$-type cluster is refluxed in water for 36 h, this results in the formation of the nanoiron molybdate $Fe_2(MoO_4)_3$ in the form of a yellow precipitate. This simple approach provides some understanding of the related Keplerate chemistry in terms of a linker–pentagon complementarity in a situation when the linkers become unstable.

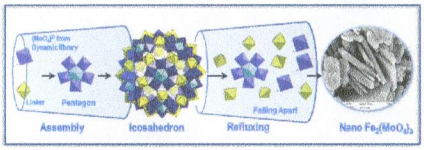


9711 S dx.doi.org/10.1021/ic4012839

**Difluorodioxophosphate-Based Hollow Hexanuclear Lanthanide(III) Clusters Decorated with Tetrathiafulvalene Ligands**

Tamyris T. da Cunha, Fabrice Pointillart,* Boris Le Guennic, Cynthia L. M. Pereira, Stéphane Golhen, Olivier Cador, and Lahcène Ouahab

The original partial hydrolysis of hexafluorophosphate in difluorodioxophosphate anions in galvanostatic condition led to the crystallization of hollow hexanuclear lanthanide(III) clusters, which are decorated with two redox-active [4,5-bis(2-pyridyl-*N*-oxidemethylthio)]-4′,5′-methyldithiotetrathiafulvene ligands.

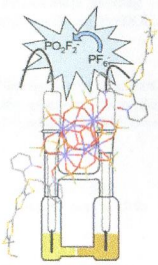

# Articles

9727 S dx.doi.org/10.1021/ic4002829

**Synthesis, Characterization, and Photophysical Properties of Heteroleptic Copper(I) Complexes with Functionalized 3-(2′-Pyridyl)-1,2,4-triazole Chelating Ligands**

Jing-Lin Chen,* Xing-Fu Cao, Jin-Yun Wang,* Li-Hua He, Zong-Yong Liu, He-Rui Wen, and Zhong-Ning Chen

A new family of luminescent monometallic Cu(I) complexes possessing functionalized 3-(2′-pyridyl)-1,2,4-triazole chelate and ancillary phosphine ligand was synthesized, and their emissive properties are well-modulated by changing the auxiliary ligand (such as a halide or phosphine), the substituent on 3-(2′-pyridyl)-1,2,4-triazole, and their environment (such as acid/base).

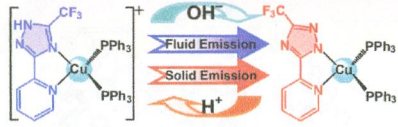


9741 S dx.doi.org/10.1021/ic400369a

**Structural Phase Transitions in a New Compound $Eu_2AgGe_3$**

Sumanta Sarkar and Sebastian C. Peter*

A new intermetallic compound $Eu_2AgGe_3$ has been synthesized using a high-frequency induction heating method. $Eu_2AgGe_3$ crystallizes in the orthorhombic $Ba_2LiSi_3$ structure type. Temperature-dependent powder XRD data and DTA hint toward a structural phase transition from orthorhombic to hexagonal above 477 K and an unusual reversible transition at around 718 K. Magnetic measurements, $^{151}$Eu Mössbauer, and X-ray absorption near-edge spectroscopic studies reveal that Eu atoms in $Eu_2AgGe_3$ exist in the divalent oxidation state.

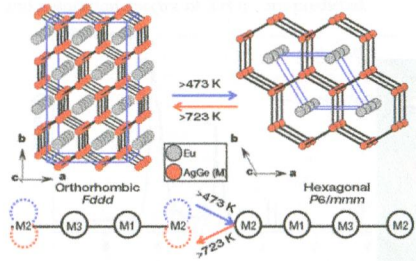


9749 S dx.doi.org/10.1021/ic4004406

**Subunit Variation to Uncover Properties of Polyazine-Bridged Ru(II), Pt(II) Supramolecules with Low Lying Charge Separated States Providing Insight into the Functioning as $H_2O$ Reduction Photocatalysts to Produce $H_2$**

Jessica D. Knoll, Samantha L. H. Higgins, Travis A. White, and Karen J. Brewer*

A detailed analysis of the redox, spectroscopic, emission, emission excitation, photophysical, and photochemical properties of the supramolecular motif $[\{(TL)_2Ru(dpp)\}_2Ru(BL')PtCl_2](PF_6)_6$ (TL = $Ph_2$phen or phen; BL′ = dpp or dpq) is reported, exhibiting complex excited state dynamics due to the spatially separated terminal Ru-based HOMO and remote BL′-based LUMO. The identity of BL′ strongly dictates the degree of photoinduced charge separation and photocatalytic water reduction, while the TL identity impacts the amount of light absorbed.

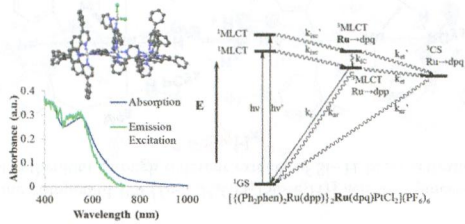

9761 dx.doi.org/10.1021/ic400474b

**Excited-State Interaction of Red and Green Perylene Diimides with Luminescent Ru(II) Polypyridine Complex**

Rajeev K. Dubey,* Marja Niemi, Kimmo Kaunisto, Kati Stranius, Alexander Efimov, Nikolai V. Tkachenko, and Helge Lemmetyinen

Three new photoactive metallo-organic donor−acceptor systems have been synthesized by the covalent attachment of Ru(II) polypyridine complex to either electron deficient (red) or electron rich (green) perylene diimide (PDI) through the bay-region. In the red-PDI-based ensemble, the excitation of either chromophore leads to the electron transfer from the Ru(II) complex to the red-PDI. In green-PDI-based ensemble, the electron transfer is observed in the opposite direction and only when the Ru(II) complex is excited.

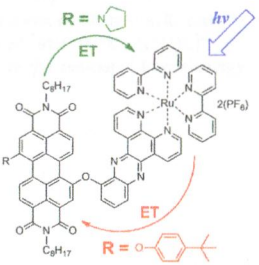


9774 dx.doi.org/10.1021/ic4016614

**Experimental and DFT Characterization of Metal-to-Ligand Charge-Transfer Excited States of (Rutheniumammine) (Monodentate Aromatic Ligand) Chromophores**

Chia Nung Tsai, Yi-Han Tian, Xuetao Shi, Richard L. Lord, H. Bernhard Schlegel,* Yuan Jang Chen,* and John F. Endicott*

Several $[Ru(NH_3)_{6-n}(MDA)_n]^{2+}$ complexes, where MDA is pyrazine or a substituted pyridine ligand, have been found to have well-characterized metal-to-ligand charge-transfer excited states in 77 K glasses. The emission spectra are broad and unstructured, the excited-state lifetimes are comparable to those of the Ru-bpy analogues, but the emission yields are very small.

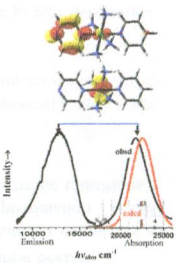


9791 dx.doi.org/10.1021/ic401447p

**Synthesis and Characterization of a Novel Sodium Transition Metal Oxyfluoride: $NaMnMoO_3F_3{\cdot}H_2O$**

Jessica Nava-Avendaño, Carlos Frontera, José A. Ayllón, Judith Oró-Solé, Premkumar Senguttuvan, and M. Rosa Palacín*

$NaMnMoO_3F_3{\cdot}H_2O$ was precipitated at low temperature, and its average crystal structure was elucidated through powder diffraction methods. Chemical analysis, infrared spectra, and effective paramagnetic moment are in agreement with the proposed formula. It consists of a stacking along the *b*-axis of layers of $MnO_4F_2$ octahedra that share corners along *a*- and *c*-directions. The large interlayer space contains water molecules, sodium ions, and the $MoO_4F_2$ octahedra (connected to the layer).

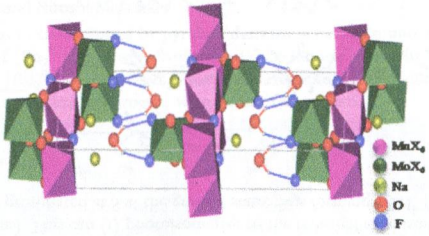

9798 dx.doi.org/10.1021/ic400703r

**Phosphinodi(benzylsilane) PhP{(*o*-$C_6H_4CH_2$)$SiMe_2H$}$_2$: A Versatile "$PSi_2H_x$" Pincer-Type Ligand at Ruthenium**

Virginia Montiel-Palma,* Miguel A. Muñoz-Hernández, Cynthia A. Cuevas-Chávez, Laure Vendier, Mary Grellier, and Sylviane Sabo-Etienne*

The new phosphinodibenzylsilane compound PhP{(*o*-$C_6H_4CH_2$)$SiMe_2H$}$_2$ acts as a pincer-type ligand capable of adopting different coordination modes at ruthenium through different extents of Si−H bond activation.

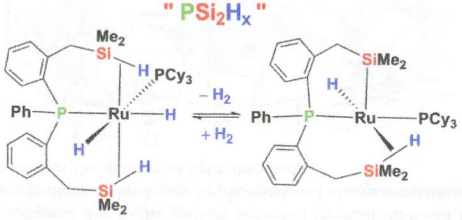


9807 dx.doi.org/10.1021/ic400735f

**Graphene/Acid Coassisted Synthesis of Ultrathin $MoS_2$ Nanosheets with Outstanding Rate Capability for a Lithium Battery Anode**

Kan Zhang, Hwan-Jin Kim, Xinjian Shi, Jeong-Taik Lee, Jae-Man Choi, Min-Sang Song,* and Jong Hyeok Park*

Ultrathin $MoS_2$ nanosheets displayed excellent rate performance for Li storage (709 $mAh{\cdot}g^{-1}$ capacity at 8320 $mA{\cdot}g^{-1}$ discharging rate) and superior charge/discharge cyclability.

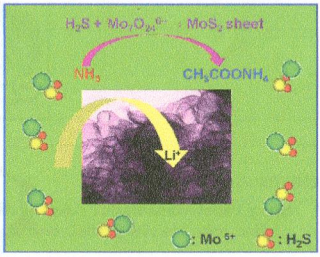


9813 dx.doi.org/10.1021/ic400774p

**Efficient Sensitization of Dye-Sensitized Solar Cells by Novel Triazine-Bridged Porphyrin−Porphyrin Dyads**

Galateia E. Zervaki, Mahesh S. Roy, Manas K. Panda, Panagiotis A. Angaridis, Emmanouel Chrissos, Ganesh D. Sharma,* and Athanassios G. Coutsolelos*

Two novel porphyrin−porphyrin dyads, the symmetrical Zn[Porph]−Zn[Porph] and unsymmetrical Zn[Porph]−$H_2$[Porph], in which the porphyrin units are covalently linked by the $\pi$-conjugated linker 1,3,5-triazine, which is functionalized by a terminal carboxylic acid, have been synthesized following a systematic synthetic approach based on the temperature-dependent reactivity of cyanuric chloride. The two novel multiporphyrin chromophores have been used for the fabrication of dye-sensitized solar cells, revealing efficient sensitization, as is evidenced by photovoltaic measurements, that resulted in power conversion efficiencies of ~4%.

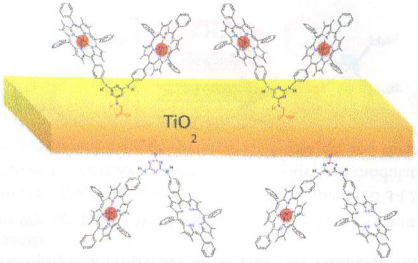

9826 (S) dx.doi.org/10.1021/ic400818t

**Excited State Properties of Diiron Dithiolate Hydrides: Implications in the Unsensitized Photocatalysis of $H_2$ Evolution**

Luca Bertini, Piercarlo Fantucci, Luca De Gioia, and Giuseppe Zampella*

According to DFT and TDDFT calculations, $H_2$ photoproduction may be due to the initial generation of a highly reactive species: the semibridging hydride (top route), which has more terminal coordination character, and a species in which one Fe−S bond is cleaved (middle route). This can (i) photoisomerize to the terminal-axial isomer (if lifetime is long enough); or (ii) after excitation decay, it can be protonated at S at the ground state, thus forming a $SH^{\delta+}/FeH^{\delta-}$ species, being able to easily release $H_2$.

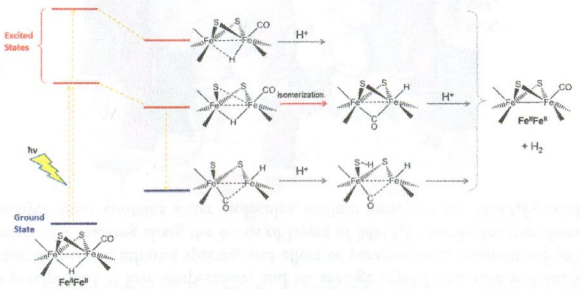


9842 (S) dx.doi.org/10.1021/ic400819f

**Syntheses, Structures, and Comparison of the Photophysical Properties of Cyclometalated Iridium Complexes Containing the Isomeric 1- and 2-(2′-pyridyl)pyrene Ligands**

Robert M. Edkins, Katharina Fucke, Michael J. G. Peach, Andrew G. Crawford, Todd B. Marder, and Andrew Beeby*

The synthesis, structures, photophysics, and electrochemistry of two isomeric, pyrene-based cyclometelated Ir complexes are compared and contrasted, supported by an in-depth (TD-)DFT study. We find that Tamm-Dancoff Approximation TD-DFT with the CAM-B3LYP functional gives the best energetic match to experiment for mixed-character electronic transitions.

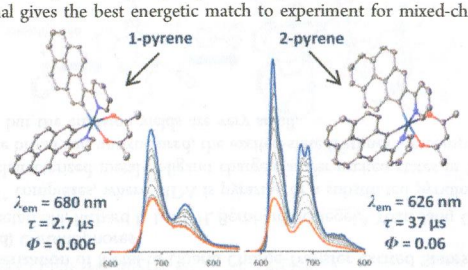

9861 S dx.doi.org/10.1021/ic401310c

**Enhanced Thermoelectric Figure of Merit in Stannite–Kuramite Solid Solutions $Cu_{2+x}Fe_{1-x}SnS_{4-y}$ ($x$ = 0–1) with Anisotropy Lowering**

Yosuke Goto,* Fumihiko Naito, Rina Sato, Keigo Yoshiyasu, Takanori Itoh, Yoichi Kamihara, and Masanori Matoba

We demonstrate the structural and thermoelectric properties of stannite–kuramite solid solutions, $Cu_{2+x}Fe_{1-x}SnS_{4-y}$ ($x$ = 0–1). Structural analysis revealed that anisotropy decreases and Cu/Sn disorder increases with an increase in $x$. The samples with $x$ = 0.8–1 exhibit degenerate conduction, whereas the Seebeck coefficient ($S$) remains relatively high, $S \approx 100\ \mu V\ K^{-1}$ for $x$ = 0.8 at 300 K.

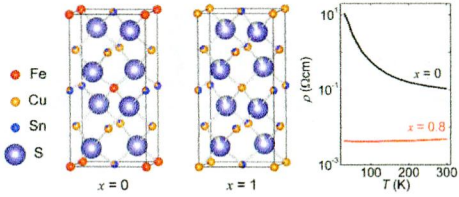


9867 S dx.doi.org/10.1021/ic4009625

**Theoretical Studies on the Photoelectron and Absorption Spectra of $MnO_4^-$ and $TcO_4^-$**

Jing Su, Wen-Hua Xu, Chao-Fei Xu, W. H. E. Schwarz,* and Jun Li*

Two experimental electron detachment energies and electronic excitation parameters of $MnO_4^-$ are well reproduced by *ab initio* methods. The photoelectron and absorption spectra of $TcO_4^-$ are predicted.

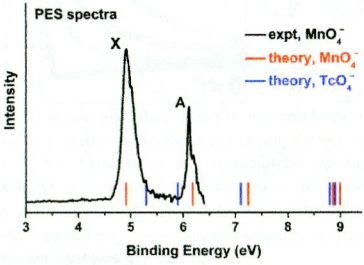


9875 S dx.doi.org/10.1021/ic400990n

**Metal Complexes (M = Zn, Sn, and Pb) of 2-Phosphinobenzenethiolates: Insights into Ligand Folding and Hemilability**

Brian M. Barry, Benjamin W. Stein, Christopher A. Larsen, Melissa N. Wirtz, William E. Geiger, Rory Waterman, and Richard A. Kemp*

New main group metal complexes containing the 2-phosphinobenzenethiolate ligands have been prepared and characterized. Sn and Pb complexes demonstrate ligand "folding" in the solid state along the P,S vector, and this folding has been explained with the help of density functional theory.

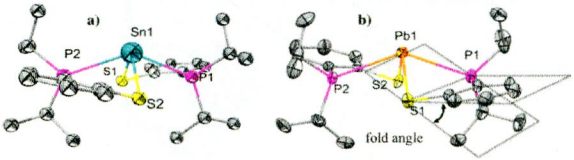

9885 dx.doi.org/10.1021/ic4010196

**Ruthenium(II) and Osmium(II) Complexes Bearing Bipyridine and the N-Heterocyclic Carbene-Based C^N^C Pincer Ligand: An Experimental and Density Functional Theory Study**

Lai-Hon Chung, Ka-Sin Cho, Jason England, Siu-Chung Chan, Karl Wieghardt, and Chun-Yuen Wong*

Spectroscopic and theoretical studies on Ru(II) and Os(II) complexes containing a neutral tridentate N-heterocyclic carbene (NHC)-based pincer ligand and a neutral 2,2′-bipyridine-type aromatic diimine in the form of $[M(C^N^C)(N^N)L]^{n+}$ support a $d\pi(RuII/OsII) \rightarrow \pi^*(N^N)$ metal-to-ligand charge transfer (MLCT) assignment to the associated lowest-energy electronic transition.

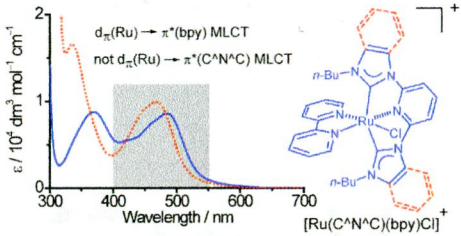


9897 dx.doi.org/10.1021/ic401022z

**Electrocatalytic $O_2$ Reduction Reaction by Synthetic Analogues of Cytochrome P450 and Myoglobin: In-Situ Resonance Raman and Dynamic Electrochemistry Investigations**

Sudipta Chatterjee, Kushal Sengupta, Subhra Samanta, Pradip Kumar Das, and Abhishek Dey*

Electrochemical $O_2$ reduction properties of imidazole and thiolate bound iron porphyrin complexes, immobilized on electrode surfaces having different electron transfer rates have been investigated using rotating ring disc electrochemistry and in situ resonance Raman spectroscopy coupled to dynamic electrochemistry.

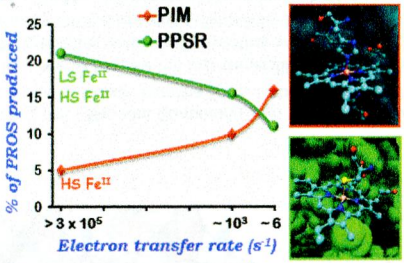


9908 dx.doi.org/10.1021/ic401030r

**Axial-Site Modifications of Paddlewheel Diruthenium(II, II) Complexes Supported by Hydrogen Bonding**

Wataru Kosaka, Naoto Yamamoto, and Hitoshi Miyasaka*

Paddlewheel-type $[Ru_2^{II,II}]$ complexes axially capped by pyridine derivatives having amino/imine groups capable of hydrogen bonding with carboxylate ligands of $[Ru_2^{II,II}]$ unit were synthesized. The intramolecular hydrogen bonding could support the ligand coordination to axial sites of $[Ru_2^{II,II}]$ unit; indeed, chain complexes with $Pd^{II}/Pt^{II}$ dithiobiuret complexes, which do not have a strong coordination ability at the imine nitrogen, were successfully derived.

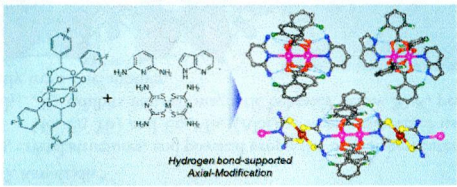

9915 S dx.doi.org/10.1021/ic4010642

**The Effect of Ligand Lipophilicity on the Nanoparticle Encapsulation of Pt(IV) Prodrugs**

Timothy C. Johnstone and Stephen J. Lippard*

A series of Pt(IV) carboxylate complexes were prepared to investigate the effect of ligand lipophilicity on encapsulation of Pt(IV) prodrugs within polymeric nanoparticles. A linear relationship exists between these parameters. The effect of increased platinum concentration on the degree of encapsulation afforded a set of optimal conditions that provide a prodrug loading maximum of 7%.

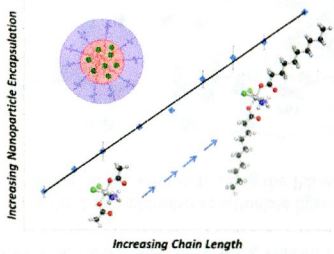


9921 S dx.doi.org/10.1021/ic401078z

**Multidimensional Network Structures and Versatile Magnetic Properties of Intermolecular Compounds of a Radical–Anion Ligand, [1,2,5]Thiadiazolo[3,4-*f*][1,10]phenanthroline 1,1-Dioxide**

Yoshiaki Shuku, Rie Suizu, Alex Domingo, Carmen J. Calzado, Vincent Robert,* and Kunio Awaga*

Diverse crystal structures and magnetic behaviors of $tdapO_2$ radical–anion salts were investigated. Single-crystal structures exhibited multidimensional network structures consisting of coordination or hydrogen bonding in addition to $\pi$ interactions. Magnetic interactions ranged from strong antiferromagnetic to ferromagnetic. Ab initio calculations suggested that the magnetic interactions were strongly governed by the $\pi$ overlaps of the radical species. Hypothetical calculations on the oxygen-removed system suggested that the oxygen atoms in $tdapO_2$ stabilize ferromagnetic interactions.

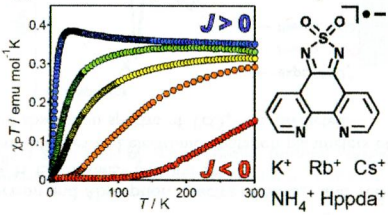

9931 dx.doi.org/10.1021/ic401659y

**Quaternary Aluminum Silicides Grown in Al Flux: $RE_5Mn_4Al_{23-x}Si_x$ (RE = Ho, Er, Yb) and $Er_{44}Mn_{55}(AlSi)_{237}$**

Nicholas P. Calta and Mercouri G. Kanatzidis*

This Article reports the synthesis, crystal structures, and physical properties of four new intermetallic compounds. Large single crystals of $RE_5Mn_4Al_{23-x}Si_x$ (RE = Ho, Er, Yb) and $Er_{44}Mn_{55}(AlSi)_{237}$ were synthesized using aluminum flux. One of the reported compounds, $Ho_5Mn_4Al_{23-x}Si_x$, exhibits unusual magnetic behavior below 20 K, perhaps as a result of two magnetic sublattices ordering independently from one another.

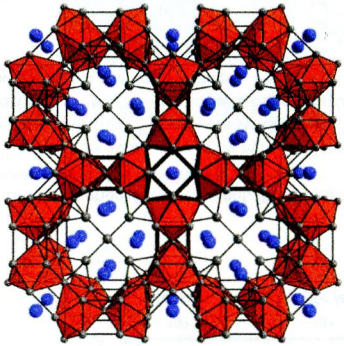

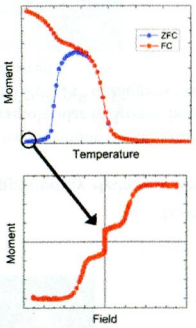


9941 dx.doi.org/10.1021/ic401139k

**Trimetallic Borohydride $Li_3MZn_5(BH_4)_{15}$ (M = Mg, Mn) Containing Two Weakly Interconnected Frameworks**

Radovan Černý,* Pascal Schouwink, Yolanda Sadikin, Katarina Stare, L'ubomír Smrčok, Bo Richter, and Torben R. Jensen

The compounds $Li_3MZn_5(BH_4)_{15}$, M = Mg or Mn, are the first trimetallic homoleptic borohydrides. They contain triangular $Zn(BH_4)_3$ and tetrahedral $Li/M(BH_4)_4$ building blocks and crystallize with a framework described as two interpenetrated **mco**-nets (**mco**-c type). It was shown by DFT calculations that, while diffraction results in a disordered M/Li site, the structure stabilizes upon maximizing locally M−M distances. Heterovalent substitution on Zn or mixed M/Li sites makes these compounds attractive as solid-state electrolyte.

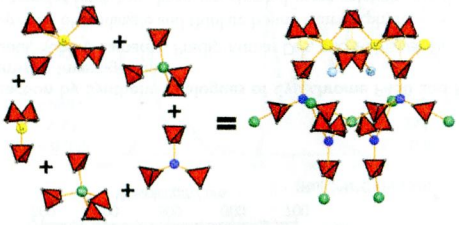

9948 S dx.doi.org/10.1021/ic401152b

**Quantitative Vibrational Dynamics of the Metal Site in a Tin Porphyrin: An IR, NRVS, and DFT Study**

Bogdan M. Leu,* Marek Z. Zgierski, Christian Bischoff, Ming Li, Michael Y. Hu, Jiyong Zhao, Steve W. Martin, Esen Ercan Alp, and W. Robert Scheidt

Experimental (nuclear resonance vibrational spectroscopy and infrared spectroscopy) and computational (density functional theory) methods were used to obtain a complete, quantitative picture of the Sn atom dynamics in tin porphyrin.

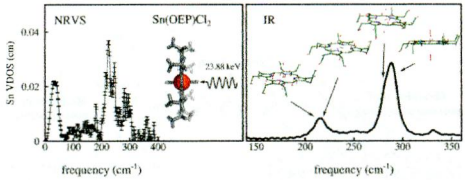


9954 S dx.doi.org/10.1021/ic401206u

**X-ray Absorption Spectroscopy Proves the Trigonal-Planar Sulfur-Only Coordination of Copper(I) with High-Affinity Tripodal Pseudopeptides**

Anne-Solène Jullien, Christelle Gateau, Isabelle Kieffer, Denis Testemale, and Pascale Delangle*

Tripodal cysteine derivatives that are highly selective chelators for copper(I) were studied by X-ray absorption spectroscopy. These architectures were demonstrated to form mononuclear copper(I) complexes with symmetric $CuS_3$ geometries and clusters based on $CuS_3$ cores, as in the high-affinity metal-sequestering metallothioneins, used by cells for the detoxification of excess copper(I). Thus, this study provides useful guidelines for the design of efficient intracellular copper(I) chelators.

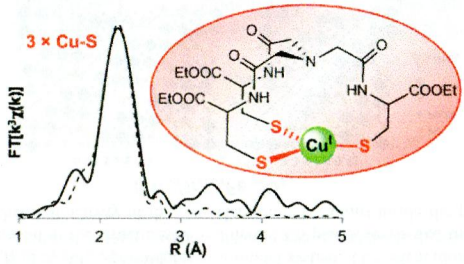


9962 S dx.doi.org/10.1021/ic401197a

**Anticancer Activity and DNA Binding of a Bifunctional Ru(II) Arene Aqua-Complex with the 2,4-Diamino-6-(2-pyridyl)-1,3,5-triazine Ligand**

Natalia Busto, Jesús Valladolid, Marta Martínez-Alonso, Héctor J. Lozano, Félix A. Jalón, Blanca R. Manzano, A. M. Rodríguez, M. Carmen Carrión, Tarita Biver, José M. Leal, Gustavo Espino,* and Begoña García*

A new Ru(II) aqua-complex, and the corresponding derivative with 9-methylguanine, have been prepared. The cytotoxic activity of the former in the cell line A2780 is noteworthy and pH-dependent. Moreover, the complex is not cross-resistant with cisplatin and reacts with DNA to give a bifunctional interaction.

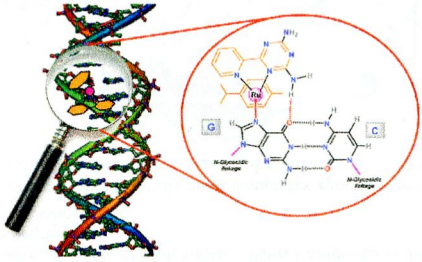

9975 dx.doi.org/10.1021/ic401232g

**Synthesis and Electrochemical Studies of Cobalt(III) Monohydride Complexes Containing Pendant Amines**

Eric S. Wiedner,* John A. S. Roberts, William G. Dougherty, W. Scott Kassel, Daniel L. DuBois, and R. Morris Bullock*

Stable $HCo^{III}$ complexes $[HCo^{III}(L2)(CH_3CN)]^{2+}$ and $[HCo^{III}(L3)(CH_3CN)]^{2+}$, containing new tetradentate phosphine ligands, were synthesized. The cyclic voltammetry of $[HCo^{III}(L2)(CH_3CN)]^{2+}$, analyzed using digital simulation, is consistent with an $E_rC_rE_r$ reduction mechanism involving reversible acetonitrile dissociation from $[HCo^{II}(L2)(CH_3CN)]^{+}$ and resulting in the formation of $HCo^{I}(L2)$. Under voltammetric conditions, $HCo^{II}$ (and possibly $HCo^{I}$) reacts with a protic solvent impurity to generate $H_2$ in a monometallic process, leading to the formation of $Co^{I}$.

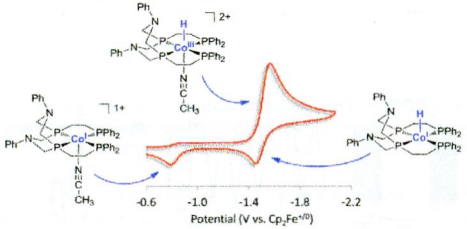


9989 dx.doi.org/10.1021/ic401857u

**Infrared Spectra and Electronic Structure Calculations for the $NUN(NN)_{1-5}$ and $NU(NN)_{1-6}$ Complexes in Solid Argon**

Lester Andrews,* Xuefeng Wang, Yu Gong, Bess Vlaisavljevich, and Laura Gagliardi

Reactions of laser-ablated U atoms with $N_2$ molecules upon co-deposition in excess argon at 4 K gave intense NUN and weaker UN infrared absorptions. Annealing produced progressions of new absorptions for the $NUN(NN)_{1,2,3,4,5}$ and $NU(NN)_{1,2,3,4,5,6}$ complexes. Electronic structure and energy and frequency calculations provide support for the identification of these complexes and characterization of the core molecules as terminal uranium nitrides.

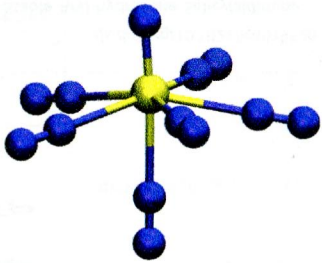

9994 dx.doi.org/10.1021/ic4012718

**Templated Non-Oxide Sol-Gel Preparation of Well-Ordered Macroporous (inverse opal) $Ta_3N_5$ Films**

Christopher F. Mallinson, Benjamin M. Gray, Andrew L. Hector,* Martyn A. McLachlan, and John R. Owen

Reactions of $Ta(NMe_2)_5$ and *n*-propylamine are shown to be an effective system for sol−gel processing of $Ta_3N_5$. Ordered macroporous films of $Ta_3N_5$ on silica substrates have been prepared by infiltration of such a sol into close-packed sacrificial templates of cross-linked 500 nm polystyrene spheres followed by pyrolysis under ammonia to remove the template and crystallize the $Ta_3N_5$.

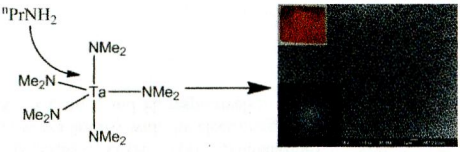

10000 S dx.doi.org/10.1021/ic401288g

**Five-Stage Near-Infrared Electrochromism in Electropolymerized Films Composed of Alternating Cyclometalated Bisruthenium and Bis-triarylamine Segments**

Chang-Jiang Yao, Yu-Wu Zhong,* and Jiannian Yao

Oxidative electropolymerization of cyclometalated bisruthenium complexes appended with triphenylamine groups produced adherent metallopolymeric films with multistep redox processes and multistage NIR electrochromism.

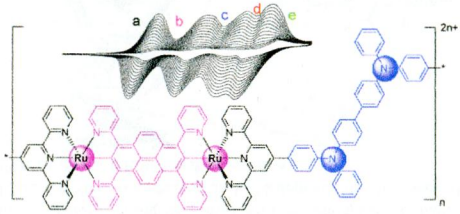


10009 S dx.doi.org/10.1021/ic4012845

**Effect of Lone-Electron-Pair Cations on the Orientation of Crystallographic Shear Planes in Anion-Deficient Perovskites**

Dmitry Batuk,* Maria Batuk, Artem M. Abakumov, Alexander A. Tsirlin, Catherine McCammon, Leonid Dubrovinsky, and Joke Hadermann

Factors affecting the structure and orientation of the crystallographic shear (CS) planes in anion-deficient perovskites are investigated using the $(Pb_{1-z}Sr_z)_{1-x}Fe_{1+x}O_{3-y}$ perovskites as a model system. The orientation of the CS planes in the system varies unevenly with $z$. A comparison of the structures with different CS planes revels that the orientation of the CS planes is governed mainly by the stereochemical activity of the lone-electron-pair cations inside the perovskite blocks.

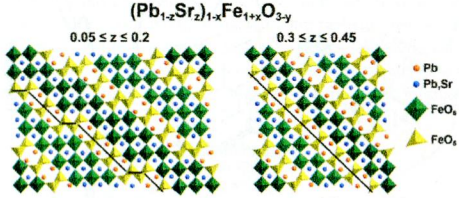


10021 S dx.doi.org/10.1021/ic401305c

**Synthesis, Structure, and Magnetic Properties of Bithiophene- and Terthiophene-Linked Manganese Metal–Organic Frameworks**

Lyndsey D. Earl, Brian O. Patrick, and Michael O. Wolf*

A series of metal–organic frameworks (MOFs) containing manganese centers and oligothiophene dicarboxylate linkers have been synthesized, including the first examples of crystallographically characterized terthiophene coordination polymers.

10031 S dx.doi.org/10.1021/ic4013284

**A Family of Layered Chiral Porous Magnets Exhibiting Tunable Ordering Temperatures**

Matteo Atzori, Samia Benmansour, Guillermo Mínguez Espallargas, Miguel Clemente-León, Alexandre Abhervé, Patricia Gómez-Claramunt, Eugenio Coronado, Flavia Artizzu, Elisa Sessini, Paola Deplano, Angela Serpe, Maria Laura Mercuri,* and Carlos J. Gómez García*

A simple change in the substituents (X) of the anilato-based bridging ligands $C_6O_4X_2^{2-}$ leads to a tuning of the ordering temperatures in the new family of hexagonal-layered porous chiral magnets $A[Mn^{II}M^{III}(C_6O_4X_2)_3]\cdot G$ ($A = [(H_3O)(phenazine)_3]^+$, $NBu_4^+$; $M^{III}$ = Cr, Fe; X = Cl, Br, I, H). $T_c$ varies linearly with the electronegativity of X from ca. 5.5 to 6.3, 8.2, and 11.0 K (for X = Cl, Br, I, and H, respectively).

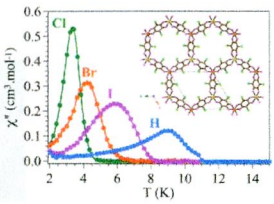


10041 S dx.doi.org/10.1021/ic401327h

**Homochiral Helical Metal–Organic Frameworks of Group 1 Metals**

Daniel L. Reger,* Andrew Leitner, Mark D. Smith, T. Thao Tran, and P. Shiv Halasyamani

Reversible single-crystal to single-crystal transformation of $Na(\mathbf{L_{ala}})(H_2O)$ (**3**, left) into $Na(\mathbf{L_{ala}})$ (**3***, right) where the bridging water (thatched oxygen atoms) of the helical rod SBU is replaced by terminal carboxylate upon removal of water.

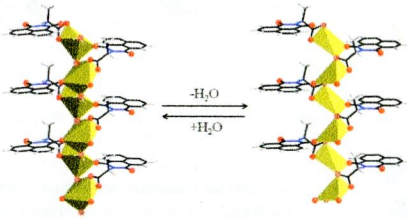


10052 S dx.doi.org/10.1021/ic4013526

**Novel Reversible $Zn^{2+}$-Assisted Biological Phosphate "Turn-On" Probing through Stable Aryl-hydrazone Salicylaldimine Conjugation That Attenuates Ligand Hydrolysis**

Olga G. Tsay, Sudesh T. Manjare, Hyungjun Kim, Kang Mun Lee, Yoon Sup Lee, and David G. Churchill*

A chemosensing ensemble, involving conjugated hydrazone [C=N—*NH*—R], greatly resists hydrolysis to allow for reversible and selective "turn-on" fluorescence sensing of ATP and PPi in aqueous media: ATP ~ PPi > ADP ≫ AMP > monophosphates ≈ others.

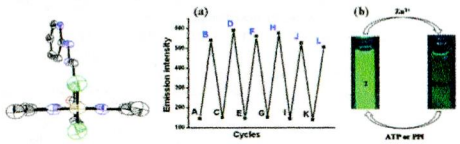

10062 Ⓢ dx.doi.org/10.1021/ic4013729

**Roles of the Lewis Acid and Base in the Chemical Reduction of $CO_2$ Catalyzed by Frustrated Lewis Pairs**

Chern-Hooi Lim, Aaron M. Holder, James T. Hynes, and Charles B. Musgrave*

In $CO_2$ reduction by frustrated Lewis pairs, the role of the Lewis acid is to activate $CO_2$ electrophilically to facilitate hydride transfer. The role of the Lewis base is to establish high concentration of the reactive $CO_2$ complex FLP·$CO_2$ that dominates the $CO_2$ reduction rate by hydride transfer.

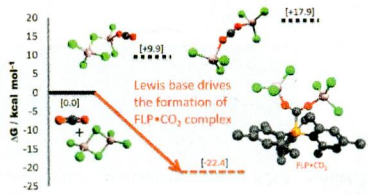


10067 Ⓢ dx.doi.org/10.1021/ic401375a

**2,2′-Bipyridine Compounds of Group 14 Elements: A Density Functional Theory Study**

Jason England and Karl Wieghardt*

The electronic structures of the known compounds $[Si(bpy)_3]^n$ ($n$ = 0, 1−, 2−), $[Si(bpy)_2Cl_2]^n$ ($n$ = 2+, 0) and $[Si(bpy)_2]^0$, plus some closely related species, were investigated by DFT and shown to contain silicon(IV) in all cases. Charge balance is attained through bpy-centered reduction. This study was also extended to include the Ge, Sn, and Pb analogues, which are hypothetical molecules in most cases, and their electronic structures assigned and feasible synthetic targets suggested.

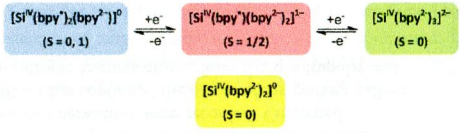


*DFT calculations show that all electronic structures contain $Si^{IV}$*

10080 Ⓢ dx.doi.org/10.1021/ic4013894

**New Selenites: Hydrothermal Syntheses, Crystal Structures, and Characterization of $Rb_3HGa_2(OH)_2(SeO_3)_4$, $Rb_3Ga_5(SeO_3)_8(HSeO_3)_2·0.5H_2O$, and $RbGa(SeO_3)_2·H_2O$**

Dong Woo Lee and Kang Min Ok*

Three new mixed-metal selenites, $Rb_3HGa_2(OH)_2(SeO_3)_4$, $Rb_3Ga_5(SeO_3)_8(HSeO_3)_2·0.5H_2O$, and $RbGa(SeO_3)_2·H_2O$, have been successfully synthesized. The open-framework material, $RbGa(SeO_3)_2·H_2O$, shows a robust ion-exchange behavior as well as reversible dehydration/rehydration properties.

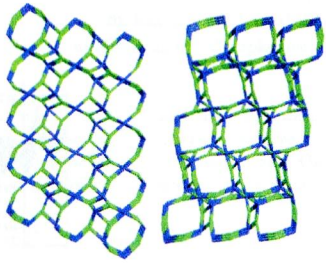

10087 S dx.doi.org/10.1021/ic4014043

**Visible-Light-Induced Photooxidation of Ruthenium(II) Complex with 2,2′-Biimidazole-like Ligand by Singlet Oxygen**

Zheng-Zheng Li, Yan-Li Niu, Hai-Yun Zhou, Hsiu-Yi Chao,* and Bao-Hui Ye*

**Ru-5** reacts with molecular oxygen under sunlight or household light at room temperature, causing the ring-opening reaction and producing **Ru-6** and **Ru-7** depending on the solvents and concentrations.

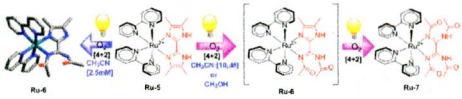


10096 S dx.doi.org/10.1021/ic401409b

**Homochiral Zinc(II) Coordination Compounds Based on In-Situ-Generated Chiral Amino Acid–Tetrazole Ligands: Circular Dichroism, Excitation Light-Induced Tunable Photoluminescence, and Energetic Performance**

Shuai-Hua Wang, Fa-Kun Zheng,* Ming-Jian Zhang, Zhi-Fa Liu, Jun Chen, Yu Xiao, A-Qing Wu, Guo-Cong Guo, and Jin-Shun Huang

We employed two pairs of new in-situ-generated chiral amino acid–tetrazole ligands in constructing homochiral Zn(II) coordination compounds: $[Zn(tzet)]_n$ (**1a** for (*S*)-tzet and **1b** for (*R*)-tzet, $H_2$tzet = *N*-[2-(1*H*-tetrazol-5-yl)ethyl]tryptophan) and $[Zn(tzep)(H_2O)_2]\cdot H_2O$ (**2a** for (*S*)-tzep and **2b** for (*R*)-tzep, $H_2$tzep = *N*-[2-(1*H*-tetrazol-5-yl)ethyl]proline), which were hydrothermally synthesized and structurally characterized by single-crystal X-ray diffraction.

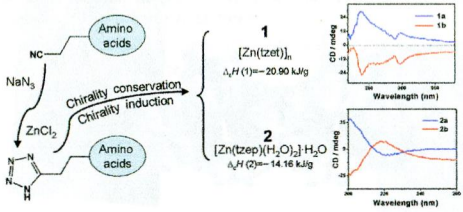


10105 dx.doi.org/10.1021/ic401419n

**In Situ XRD Study of $La_2Ni_7H_x$ During Hydrogen Absorption–Desorption**

Kenji Iwase,* Kouji Sakaki, Yumiko Nakamura, and Etsuo Akiba

$La_2Ni_4$ cell and $LaNi_5$ cell volumes in orthorhombic hydrides during absorption–desorption processes are investigated.

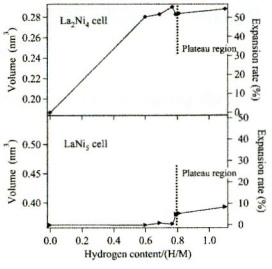

10112 S dx.doi.org/10.1021/ic401455c

**Substantial Cd–Cd Bonding in $Ca_6PtCd_{11}$: A Condensed Intermetallic Phase Built of Pentagonal $Cd_7$ and Rectangular $Cd_{4/2}Pt$ Pyramids**

Fakhili Gulo, Saroj L. Samal, and John D. Corbett*

The new trail-breaking compound Ca6PtCd11 has been synthesized and its structural and bonding properties investigated. This unusual phase features an unprecedented degree of cadmium aggregation, including linear chains, novel Cd7 PBP aggregates, and edge-shared chains of PtCd4/2 square pyramids. Manifestations of this chemistry elsewhere has evidently been precluded in earlier work by the inclusion of larger amounts of the strong d-metal bonding Au or Pt. Under the right conditions Cd seems quite effective as an open s,p-band metal.

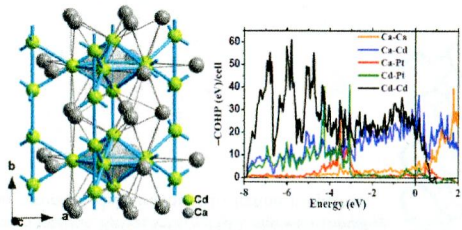


10119 S dx.doi.org/10.1021/ic401521m

**On the Track to Silica-Supported Tungsten Oxo Metathesis Catalysts: Input from $^{17}O$ Solid-State NMR**

Nicolas Merle, Guillaume Girard, Nicolas Popoff, Aimery De Mallmann, Yassine Bouhoute, Julien Trébosc, Elise Berrier, Jean-François Paul, Christopher P. Nicholas, Iker Del Rosal, Laurent Maron,* Régis M. Gauvin,* Laurent Delevoye,* and Mostafa Taoufik*

The grafting of an oxochlorotrisalkyl tungsten derivative on $SiO_{2\text{-}700}$ affords a well-defined alkene metathesis precatalyst via W–Cl cleavage, as shown by spectroscopic and theoretical investigations. $^{17}O$ MAS NMR spectra of a series of related $^{17}O$-labeled molecular and supported tungsten oxo derivatives were recorded. Combined experimental and theoretical NMR studies confirmed the nature of the grafting pathway, thanks to highly characteristic anisotropic features arising from the quadrupolar and chemical shift interactions.

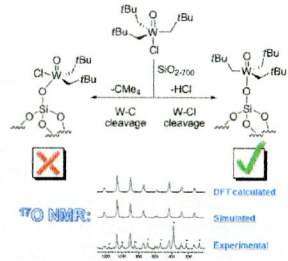


10131 S dx.doi.org/10.1021/ic401531r

**Luminescence of $[Ru(bpy)_2(dppz)]^{2+}$ Bound to RNA Mismatches**

Anna J. McConnell, Hang Song, and Jacqueline K. Barton*

The luminescence of *rac*-$[Ru(bpy)_2(dppz)]^{2+}$ (bpy =2,2′-bipyridine and dppz = dipyrido[3,2-*a*:2′,3′-*c*]phenazine) was explored in the presence of RNA oligonucleotides containing a single RNA mismatch (CA and GG) in order to develop a probe for RNA mismatches.

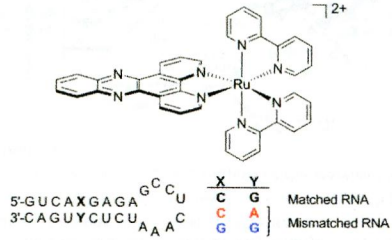

10137 dx.doi.org/10.1021/ic401573d

**Dicopper(II) and Dizinc(II) Complexes with Nonsymmetric Dinucleating Ligands Based on Indolo[3,2-*c*]quinolines: Synthesis, Structure, Cytotoxicity, and Intracellular Distribution**

Michael F. Primik, Simone Göschl, Samuel M. Meier, Nadine Eberherr, Michael A. Jakupec, Éva A. Enyedy, Ghenadie Novitchi, and Vladimir B. Arion*

Dicopper(II) and dizinc(II) complexes $[Cu_2(^{MeOOC}L^{COO})(CH_3COO)_2]$ (**1**) and $[Zn_2(^{MeOOC}L^{COO})(CH_3COO)_2]$ (**2**) were synthesized by reaction of $Cu(CH_3COO)_2{\cdot}H_2O$ and $Zn(CH_3COO)_2{\cdot}2H_2O$ with a new nonsymmetric dinucleating ligand $^{EtOOC}HL^{COOEt}$ prepared by condensation of 6-hydrazinyl-11*H*-indolo[3,2-*c*]quinoline with diethyl-2,2′-((3-formyl-2-hydroxy-5-methylbenzyl)azanediyl)diacetate.

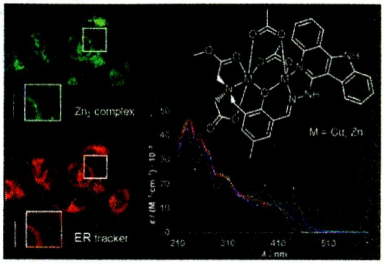


10147 dx.doi.org/10.1021/ic401576q

**Interplay between Chemical Composition and Cation Ordering in the Magnetism of Ni/Fe Layered Double Hydroxides**

Gonzalo Abellán, Eugenio Coronado,* Carlos Martí-Gastaldo,* Joao Waerenborgh, and Antonio Ribera

We report the synthesis of a family of ferrimagnetic NiFe layered double hydroxides (LDHs) with a variable $Ni^{2+}/Fe^{3+}$ in-plane composition of $[Ni_{1-x}Fe_x(OH)_2](CO_3)_{x/2}{\cdot}yH_2O$ ($x$ = 0.20, 0.25, and 0.33) by following a modified homogeneous precipitation.

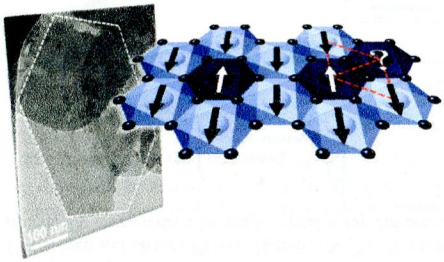

10158 dx.doi.org/10.1021/ic401603y

**Zirconium Complexes Supported by an *N*-Perfluoro-Arylated Diamidopyridyl Ligand: Synthesis of Hydrazinediido Complexes**

Solveig A. Scholl, Gudrun T. Plundrich, Hubert Wadepohl, and Lutz H. Gade*

In this work we report the synthesis of a pentafluorophenyl substituted $[N_2^{PRP}N_{py}]^{2-}$ ligand, its transformation upon reaction with $[Zr(NMe_2)_4]$, and the stepwise synthesis of hydrazinediido–zirconium complex.

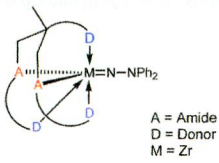

10167 dx.doi.org/10.1021/ic401646t

**Hexagonal Crown-Capped Zinc Oxide Micro Rods: Hydrothermal Growth and Formation Mechanism**

Lijing Zhang, Xiaomiao Liu, Chong Geng, Huajing Fang, Zhipeng Lian, Xiaoqing Wang, Dezhong Shen, and Qingfeng Yan*

Hexagonal crown-capped ZnO micro rods were successfully prepared by a facile low-temperature hydrothermal method. The as-prepared ZnO micro rods are 4.4−5.2 $\mu$m in length and 2.4−3.6 $\mu$m in diameter, possessing a single-crystal hexagonal structure. The morphology evolution and structure changes were tracked during hydrothermal growth by field-emission scanning electron microscopy and X-ray diffraction, respectively. A three-stage growth mechanism of the hexagonal crown-capped ZnO micro rods was proposed and further verified by a growth solution renewal experiment.

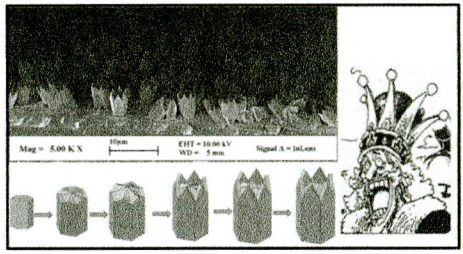

10176 dx.doi.org/10.1021/ic401648b

**Hard and Soft Metal Complexes of Calix[4]-*bis*-monothiacrown-5: X-ray and NMR Studies of Discrete Homodinuclear Complexes and a Heteromultinuclear Network**

Ja-Yeon Kim, In-Hyeok Park, Jai Young Lee, Joon-Hwa Lee, Ki-Min Park, and Shim Sung Lee*

A hard/soft heterometallic coordination of calix[4]-*bis*-monothiacrown-5 (**L**) is reported. Reaction of **L** with KI in the presence of $HgI_2$ afforded a 2D network $[K_2LHg_4I_{10}]_n$ with the exocyclic mercury(II) iodide cluster backbone cross-linked by the endocyclic dipotassium(I) complex unit.

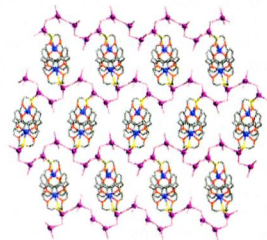

10183 dx.doi.org/10.1021/ic401667v

**Four-Electron Oxidative Dehydrogenation Induced by Proton-Coupled Electron Transfer in Ruthenium(III) Complex with 2-(1,4,5,6-Tetrahydropyrimidin-2-yl)phenolate**

Ryoji Mitsuhashi,* Takayoshi Suzuki,* and Yukinari Sunatsuki

Seven $[Ru(O\text{-}N)(bpy)_2]^{n+}$ (O-N = unsymmetrical bidentate phenolate type ligand, bpy = 2,2′-bipyridine) complexes were characterized by X-ray crystallography, cyclic voltammetry, $^1H$ NMR, and UV−vis spectroscopy. Two-electron oxidative dehydrogenation was observed for the ruthenium(III) complex with 2-(2-imidazolinyl)phenolate upon addition of base. On the other hand, four-electron oxidative dehydrogenation was observed in the 2-(1,4,5,6-tetrahydropyrimidin-2-yl)phenolate analog.

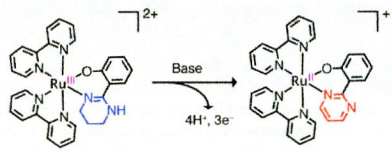


*Four-electron Oxidative Dehydrogenation*

10191 S dx.doi.org/10.1021/ic401705j

**Synthesis and Structural Characterization of Hydrolysis Products within the Uranyl Iminodiacetate and Malate Systems**

Daniel K. Unruh, Kyle Gojdas, Erin Flores, Anna Libo, and Tori Z. Forbes*

Isolation and characterization of oligiomeric hydrolysis products, including a uranyl unidecamer carbonato species, from near-neutral aqueous solutions.

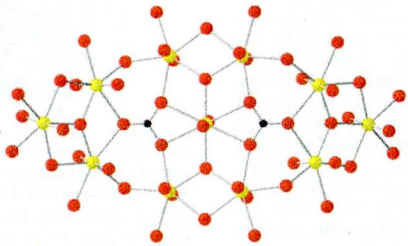

10199 S dx.doi.org/10.1021/ic4017678

**Water-Soluble $Tb^{3+}$ and $Eu^{3+}$ Complexes with Ionophilic (Ionically Tagged) Ligands as Fluorescence Imaging Probes**

Julia R. Diniz, José R. Correa, Daniel de A. Moreira, Rafaela S. Fontenele, Aline L. de Oliveira, Patrícia V. Abdelnur, José D. L. Dutra, Ricardo O. Freire, Marcelo O. Rodrigues,* and Brenno A. D. Neto*

Endoplasmic reticulum could be selectively stained using a new water-soluble terbium complex. The new complex showed complete solubility in aqueous media at room temperature as a consequence of using a task-specific ionic liquid as an ionophilic ligand (ionically tagged) bearing an imidazolium cation with a hydrophilic anion (chloride).

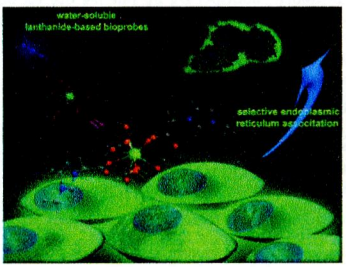


10206 dx.doi.org/10.1021/ic401805x

**Effect of Electrostatic and Size on Dopant Occupancy in Lithium Niobate Single Crystal**

Keyan Li, Congying Kang, and Dongfeng Xue*

Site occupancies of metal ions in the whole periodic table in $LiNbO_3$ single crystal are determined by considering the electrostatic and size effects of cations on the structural stability of doped $LiNbO_3$ crystals.

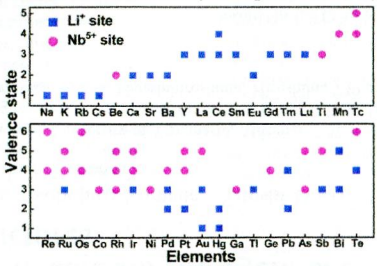

dx.doi.org/10.1021/ic40200

**Extended Ni(III) Oxyhalide Perovskite Derivatives: $Sr_2NiO_3X$ ($X$ = F, Cl)**

Yoshihiro Tsujimoto,* Kazunari Yamaura, and Tetsuo Uchikoshi

Extended layered oxyhalide compounds, $Sr_2NiO_3X$ ($X$ = F, Cl), with the square pyramidal coordination around the trivale nickel ions in the low spin state ($S = 1/2$), are successfully synthesized by a high-pressure and high-temperature reaction. Bo these compounds crystallize in the $n = 1$ Ruddlesden–Popper type structure, but the difference of halogen anions incorporated dictate the anion-site ordering patterns and the magnetic ground states.

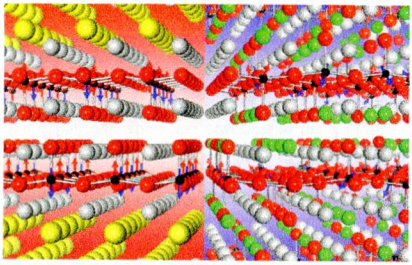

Supporting Information available via online article